BUTTERWORTH HEINEMANN

Polymer Vol. 36 No. 7, pp. 1425-1434, 1995

0032-3861/95/$10.00+0.00

Phase separation in PMMA/silica sol–gel systems

Kátia Fraga Silveira, Inez Valéria P. Yoshida and Suzana Pereira Nunes*
University of Campinas, Institute of Chemistry, 13081 Campinas-SP, Brazil
(Received 7 February 1994; revised 26 September 1994)

The mechanism of phase separation of sol–gel alkoxy-derived silica systems obtained by acid catalysis in the presence of poly(methyl methacrylate) (PMMA) and tetrahydrofuran was investigated by light scattering. Spinodal decomposition (SD) was confirmed for systems with intermediate PMMA/alkoxy compositions occurring with a simultaneous viscosity increase. The initial stages of phase separation followed the linear theory proposed by Cahn. For systems with low PMMA content, a behaviour typical of nucleation and growth was detected. In this case gelation took place after demixing. The morphology of the final PMMA/silica hybrid material was investigated by scanning and transmission electron microscopy with element-specific analysis. A matrix/disperse domains morphology was also verified for systems which demixed by SD, indicating that phase coarsening occurs. A micellar/lamellar microstructure was observed inside the separated phases.

(Keywords: phase separation; PMMA/silica; sol–gel)

INTRODUCTION

Polymer composites have an undeniable technological importance and have been widely investigated[1]. The introduction of inorganic fillers to a polymer matrix increases its strength and stiffness and sometimes creates characteristics of a totally different material. In this two-phase system, the size of the inorganic particles strongly influences the final properties which are also controlled by the interfacial interactions between matrix and fillers. In many applications, the improvement of mechanical properties is only a first consideration and characteristics such as transparency and specific permeability are also required. Recently a new class of inorganic/organic 'composites' has become very attractive in the development of new materials. The possibility of creating the inorganic phase '*in situ*' by a sol–gel process increased the chances and mechanisms of morphology control and allowed the preparation of 'ceramers', inorganic/organic hybrids with a good dispersion even at the molecular level[2–7]. These materials have a potential application for contact lenses[3,8], membranes[9], non-linear optics[10,11], coatings[3,11], etc.

In most cases of sol–gel hybrid preparation, the inorganic phase is grown from hydrolysis–condensation reactions of alkoxysilanes, mainly tetramethoxy- (TMOS) and tetraethoxysilanes (TEOS). The following variations may be considered: (1) inorganic network formation in a solution containing organic polymers[12–14]; (2) inorganic network formation in a solution containing functionalized organic polymers, which allows covalent bonds between the phases[2,3]; (3) simultaneous growth of the inorganic network and the organic polymer[6]; (4) simultaneous growth of an inorganic/organic interpenetrating polymer network[15,16]; and (5) growth of an inorganic/organic polymer network with covalent bonds between both parts[5,8]. The first variation is probably the most simple procedure, but normally leads to a phase-separated material. In the recent literature, hybrid preparation in this way has been described using poly(vinyl alcohol) (PVA)[12], poly(acrylic acid)[13,14], poly(methyl methacrylate) (PMMA)[17,18], poly(vinyl pyrrolidone) (PVP)[18], polydimethylsiloxane (PDMS), poly(ethylene oxide) (PEO)[19] and Nafion[20]. A large diversity of morphology can be obtained. Very few studies have been published[13,14] investigating the mechanism of phase separation in these systems. Light scattering seems to be a very suitable method for this purpose, which has been widely applied to polymer blends and polymer solutions[21,22]. In this work the phase separation of a TEOS/PMMA system is investigated by light scattering during the sol–gel reaction and solvent evaporation. The morphology of the final hybrid product is investigated by scanning and transmission electron microscopy with element contrast for different polymer compositions and molecular weights.

EXPERIMENTAL

Materials

Both TEOS and PMMA were supplied by Aldrich. PMMA with different molecular weights was used: PMMA (low) with $M_w = 97\,000\,g\,mol^{-1}$ and $M_w/M_n = 2.7$ and PMMA (high) with $M_w = 133\,000\,g\,mol^{-1}$ and $M_w/M_n = 3.3$. Tetrahydrofuran (THF) was supplied by Merck and hydrochloric acid (HCl) was purchased from Labsynth.

Sample preparation

Inorganic/organic hybrids were prepared by a sol–gel process with condensation/hydrolysis of TEOS in a THF/PMMA solution. The reaction mechanism is well

* To whom correspondence should be addressed

described in the literature[23]. An inorganic network is formed as the result of three reactions:

1. Hydrolysis

$$Si(OCH_2CH_3)_4 + H_2O \rightarrow (CH_3CH_2O)_3Si\text{–}OH + CH_3CH_2OH$$

2. Alcohol condensation

$$Si(OCH_2CH_3)_4 + (CH_3CH_2O)_3Si\text{–}OH \rightarrow (CH_3CH_2O)_3Si\text{–}O\text{–}Si(OCH_2CH_3)_3 + CH_3CH_2OH$$

3. Water condensation

$$(CH_3CH_2O)_3Si\text{–}OH + (CH_3CH_2O)_3Si\text{–}OH \rightarrow H_2O + (CH_3CH_2O)_3Si\text{–}O\text{–}Si(OCH_2CH_3)_3$$

Finally, a SiO_2 network is formed:

$$Si(OCH_2CH_3)_4 + 2H_2O \rightarrow SiO_2 + 4CH_3CH_2OH$$

Hydrolysis is much faster in the presence of acidic or basic catalysts. A general trend in sol–gel processes using pure alkoxy (without the organic polymer) is that acid-catalysed hydrolysis with low water/Si ratios produces a weakly branched polymeric network, whereas base-catalysed hydrolysis gives highly branched 'colloidal' particles, as reported by Brinker[23]. Excess water may favour depolymerization. In the experiments described here, different volumes of TEOS were carefully added to a continuous mixing 10 wt% THF/PMMA solution. A 0.15 M HCl aqueous solution was then dropped into the clear PMMA solution, always keeping a 4:1 molar water/TEOS stoichiometric proportion. The solution was further stirred for 16 h at room temperature (25°C) and transferred to a closed Petri dish. The reaction was allowed to continue for 24 h. The dish was then opened and the solvent was slowly evaporated at room temperature.

Light scattering

The equipment for light scattering measurements was mounted in the laboratory using a He–Ne laser ($\lambda = 633$ nm) as the radiation source and a photodiode as detector, which was connected to a microcomputer by an A/D interface. A small Bosch DHP 12 V motor provided a constant variation of the detector relative to the laser. The detector angle was previously calibrated by crossing two lasers at a defined angle. The scattering pattern was recorded with the sample in a Petri dish, during solvent evaporation at room temperature ($T = 23$°C).

Scanning electron microscopy

The samples were fractured in liquid nitrogen and coated with gold by sputtering. Secondary electron images were obtained in a JEOL T-300 scanning electron microscope. X-ray mapping for silicon was performed with an energy dispersive spectrometer.

Transmission electron microscopy

Samples were cut at −20°C with a diamond knife in an Ultracut Reichert-Jung microtome and observed in a Zeiss CEM-902 transmission microscope. The microscope has a spectrometer which uses inelastic electrons to form element specific images[24]. When the electron beam passes through the sample, interaction with electrons of different elements results in characteristic energy losses. A prism-mirror system deflects electrons with different energies to different angles so that only electrons with a well defined energy can be selected. If only elastic electrons are chosen ($\Delta E = 0$) a bright field image with reduced chromatic aberration is obtained. When monochromatic inelastic electrons are selected, electron spectroscopic images (ESI) are formed showing the local concentration of a particular element (bright regions). For the inorganic/organic system investigated here images were obtained first at the energy loss $\Delta E = 1855$ eV right above the ionization edge of silicon and at $\Delta E = 1810$ eV, below it. The subtraction of the second image eliminated the background. Micrographs were also obtained at $\Delta E = 295$ eV and $\Delta E = 270$ eV for carbon specific images. The electron energy loss spectrum (EELS) was also obtained with the microscope photomultiplier electron detector.

RESULTS AND DISCUSSION

In the systems investigated here the co-occurrence of gelation by a reactive process and phase separation is of fundamental importance to the final product, an inorganic/organic glass. The glass could be seen as a semi-interpenetrating polymer network, with PMMA dispersed in a crosslinked silica structure with different degrees of segregation.

Phase separation mechanisms

Phase separation is well described in the literature for polymer solutions and polymer blends[21–22,25], in which the one-phase region of the phase diagram and the metastable and unstable regions are limited by the binodal and the spinodal curves. Two mechanisms are normally considered for the phase separation: nucleation and growth (NG) and spinodal decomposition (SD). The NG mechanism is preferable for quenching into the metastable phase region, between the binodal and the spinodal. Nucleation initiates with local density or concentration fluctuations, forming nuclei with well defined interfaces. It requires an activation energy, which depends on the interfacial energy for creating the nuclei. The process evolution with diffusion of macromolecules into the nucleated domains is spontaneous. The nucleus composition is constant. The morphology observed during a NG phase separation is, from the early to the later stages, the droplet/matrix type. On the other hand, SD is the phase separation mechanism that occurs for quenchings into the unstable region enclosed by the spinodal. Delocalized concentration fluctuations initiate spontaneously with a predominant wavelength which is constant at the very early stages and depends on the quench depth. The fluctuation wavelength increases in the intermediate stages and phase coalescence is observed in the late stages. If coalescence can be avoided, a three-dimensional co-continuous morphology is obtained leading to outstanding mechanical properties of polymer blends as described in the literature[25,26].

Light scattering theory for phase separation

Using light scattering experiments, as described by Hashimoto[22], the NG mechanism of phase separation can be recognized by a monotonic decrease of light intensity with scattering angle. When phase separation follows the SD mechanism a scattering halo is detected, which in the early stages at least follows the linear theory proposed by Cahn[27]. The SD theory is applied to each

polymeric system when the dominant fluctuation wavelength is much larger than the individual polymer coils. Linearity is expected only in the early stages of phase separation and in systems where the contribution of random thermal noise is not significant.

Concentration fluctuations with different wavelengths contribute to light scattering at different angles, θ. Each angle is related to a wavenumber q:

$$q=(4\pi/\lambda)\sin(\theta/2) \quad (1)$$

where λ is the wavelength of the incident light.

The wavelength of the predominant fluctuation in the system, d, can be estimated from the wavenumber, q_m, at the maximum scattered light intensity:

$$d=2\pi/q_m \quad (2)$$

At a constant temperature quenching depth the fluctuation amplitude increases during the phase separation. In the early stages, the scattered light intensity exponentially increases with time for each q, without any shift of q_m. In its intermediate and later stages phase separation deviates from the linear theory and coarsening is observed.

The amplitude growth rate of fluctuations with different wavelengths, $R(q)$, can be estimated from:

$$I(q,t)\sim\exp[2R(q)t] \quad (3)$$

$R(q)$ depends on both the thermodynamic condition and on the system mobility. From $R(q)$ values at different q, an apparent diffusion coefficient, D_{app}, can be estimated:

$$D_{app}=\lim_{q\to 0}[2R(q)/q^2] \quad (4)$$

D_{app} expresses how fast the phase separation takes place. It is directly proportional to the mobility in the system but also depends on the thermodynamic conditions.

$$D_{app}=D(\chi-\chi_s)/\chi_s \quad (5)$$

D is the self-diffusivity, χ is the interaction parameter at a certain condition and χ_s is χ at the spinodal. At the spinodal temperature for a binary system there is a critical slowing down and $D_{app}=0$.

Isothermal phase separation: solvent evaporation and reactive processes

Most of the papers on phase separation mechanisms consider an isothermal process after a temperature quenching into the two-phase region. Here phase separation occurs in a more complex situation: it is induced by (1) the TEOS reaction and (2) simultaneous solvent evaporation. An isothermal phase separation in a non-reactive system by solution casting may be considered as a two-step process: an isothermal quenching in a one-phase condition leading to the final composition, followed by a one-step temperature jump into the two-phase region at constant composition. However, a system actually enters the two-phase region by casting with a rather slow solvent evaporation. The temperature jump step could be then better depicted by a series of successive quenchings.

When phase separation is induced by a reactive process, the phase diagram continuously changes. However, a convenient way of modelling the demixing process has been to consider successive increases in quench depth in a constant phase diagram. Ohnaga *et al.*[28,29], by computer simulations based on the Cahn–Hilliard non-linear diffusion equation, showed how concentration fluctuations grow in such a system. They are highly dependent on the quench rate. However, the applied kinetic equation includes a term which is identical to the equation derived by the linearized SD theory proposed by Cahn and this linear term may dominate in many situations, allowing the use of simple considerations for discussing the demixing behaviour of rather complex systems.

Co-occurrence of gelation and phase separation in a sol–gel process

In addition to phase separation, in the system investigated here, solvent evaporation and the reactive process may lead to gelation. A classical description of gelation was presented by Flory[30] and Stockmayer[31], who considered the random formation of bonds between adjacent nodes of an infinite tree as a model for polycondensation of bi- and polyfunctional monomers. Many new concepts, such as the fractal dimension[32], have been introduced since then to give a more accurate vision of the gelation phenomena. A comprehensive theory was proposed by de Gennes[33] to explain a polycondensation reaction. He used the percolation model, where bonds are randomly placed in a d-dimensional lattice. A special consideration is necessary when monomers are mixed with a solvent. In this case, as the monomers become attached together by chemical links, they tend to form clusters, which could eventually segregate and precipitate. There is then competition between gelation and segregation. Analogous to a phase separation process occurring by temperature variation, demixing induced by chemical reaction at constant temperature may be represented by a phase diagram in which the reaction progress is represented by an equivalent temperature, T_{eq}, which is the relation between an attractive interaction energy (corresponding to the covalent bonding) and the correlation strength between monomers, β ($\beta=0$ before the reaction begins and increases as it progresses). T_{eq} decreases from infinity to low values as the chemical reaction goes on. These concepts were used here to describe the co-occurrence of phase separation and gelation during PMMA/TEOS hybrid formation by the sol–gel process, as shown in *Figure 1*. In this case, T_{eq} takes into account both the effects of the reaction progress but also the β increase due to solvent evaporation. ϕ is the mer concentration in the dilute medium, which also varies as the solvent evaporates.

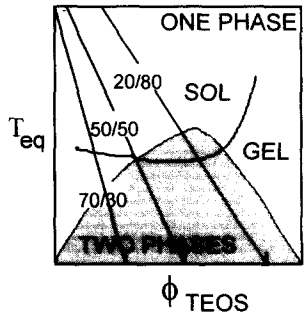

Figure 1 Co-occurrence of phase separation and gelation during the sol–gel process

Phase separation in the PMMA/TEOS system

During PMMA/TEOS hybrid formation, TEOS is initially homogeneously dispersed in the THF/PMMA solution. As the hydrolysis/condensation reaction goes on, the inorganic SiO_2 network is formed, still swollen by THF/PMMA. The growth of the SiO_2 network is entropically unfavourable towards miscibility and the enthalpic interaction between the PMMA segments and the inorganic component also deteriorates, whilst the OH– and CH_3CH_2O– group content in the network progressively decreases. The THF functions as a co-solvent swelling the growing network and diluting the unfavourable interaction between SiO_2 and PMMA segments. Even after several days of reaction no phase separation was observed if no solvent was allowed to evaporate.

Phase separation was observed for all PMMA/TEOS investigated compositions: from 20/80 to 70/30 with PMMA of different molecular weights. For 20/80 low molecular weight PMMA/TEOS solutions, demixing was faster, followed by an observable increase in viscosity. For 50/50 solutions, demixing was observed with an almost simultaneous increase in viscosity. In both cases, glasses with high opacity were obtained after solvent evaporation, while for 70/30 solutions a translucent material was produced. In solutions with high molecular weight PMMA, the initial viscosity was higher. In *Figure 1*, a gelation curve crosses the phase separation curve twice. If the system attains the gelation condition before the phase separation, it may even be inhibited. If the mobility is low enough, only on a local scale (sizes comparable to the distance between crosslinks), micro-phase separation may take place.

Scattering halos were observed during demixing of systems with PMMA (low)/TEOS composition between 50/50 and 60/40. In 20/80 and 70/30 systems, no halo was detected, only an increase of scattered light intensity at low angles with time was observed and the intensity monotonically decreased with increasing angle. For high molecular weight PMMA, a halo was detected even in 70/30 PMMA/TEOS solutions. The evolution of the scattering pattern during demixing is shown in *Figure 2* for different systems. Time = 0 s corresponds to the first indication of phase separation, typically ~ 10 h of solvent evaporation with an open Petri dish. *Figure 3* shows a plot of relative scattered light intensity (I/I_0) as a function of time for the 50/50 PMMA (low)/TEOS system. Similar plots were obtained for the 60/40 (low) and 50/50 (high) systems, confirming that when a halo was observed, the I/I_0 growth at each angle was exponential in the early stages and stopped after a certain time. The exponential increase is typical for spinodal decomposition. For each of the systems with SD phase separation, plots of $R(q)/q^2$ as a function of q^2 were obtained, as shown in *Figure 4* for the 50/50 (low) system and apparent diffusion coefficients were calculated using equation (4). D_{app} is an indication of how fast the phase separation proceeds. Here the D_{app} values shown in *Table 1* may be used to reflect the main differences in the system's mobility when phase separation begins.

As shown in *Figure 3*, non-linear terms become important as phase separation goes on. *Figure 5* shows

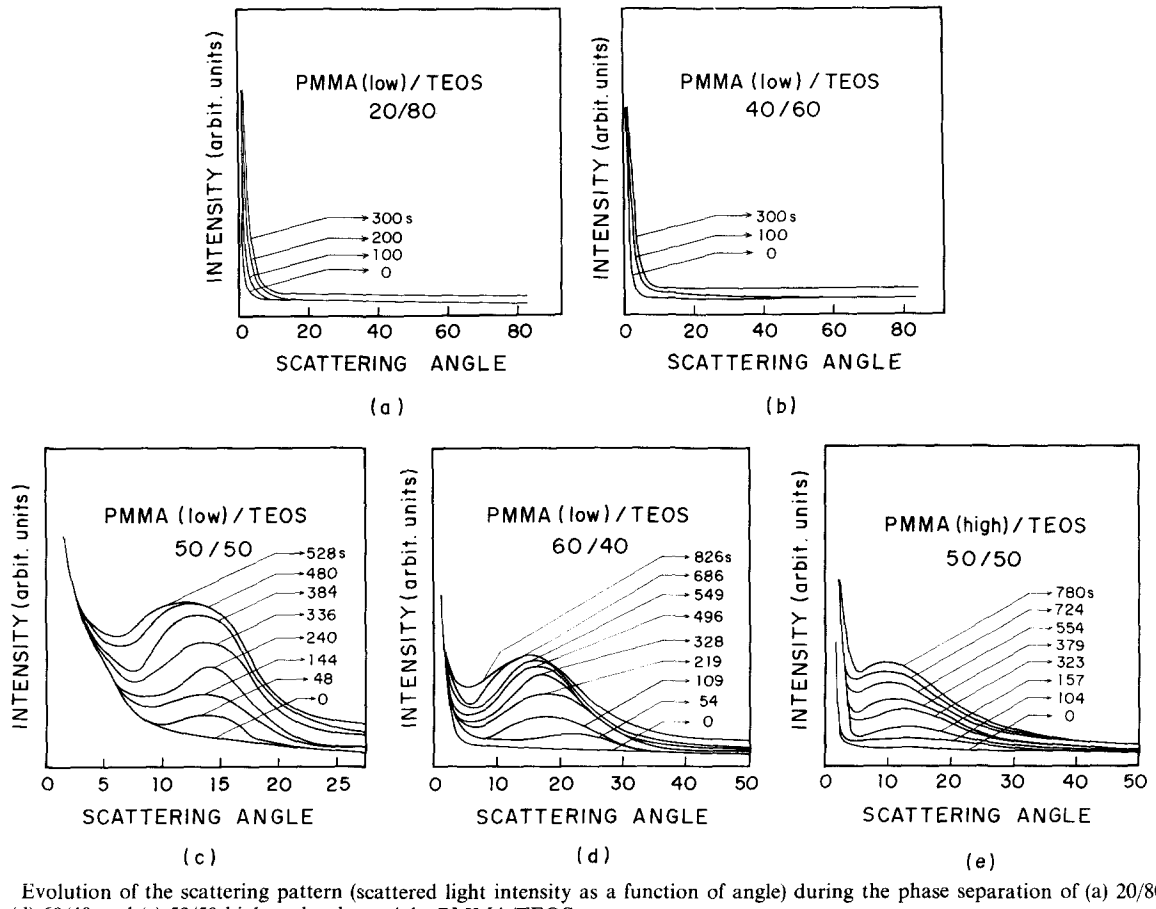

Figure 2 Evolution of the scattering pattern (scattered light intensity as a function of angle) during the phase separation of (a) 20/80, (b) 40/60, (c) 50/50, (d) 60/40 and (e) 50/50 high molecular weight PMMA/TEOS

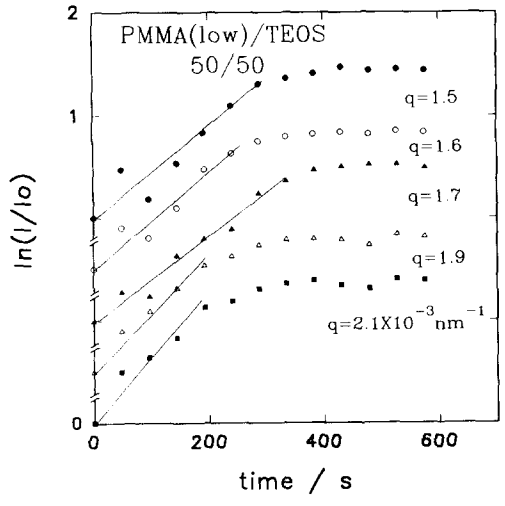

Figure 3 Relative scattered light intensity as a function of time at different angles for the 50/50 low molecular weight PMMA/TEOS system

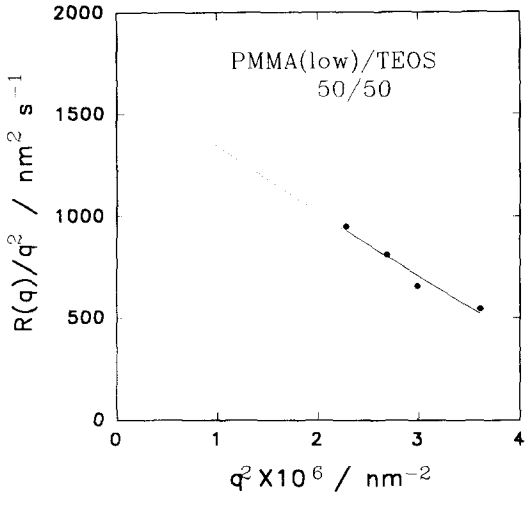

Figure 4 $R(q)/q^2$ as a function of q for the 50/50 low molecular weight PMMA/TEOS system

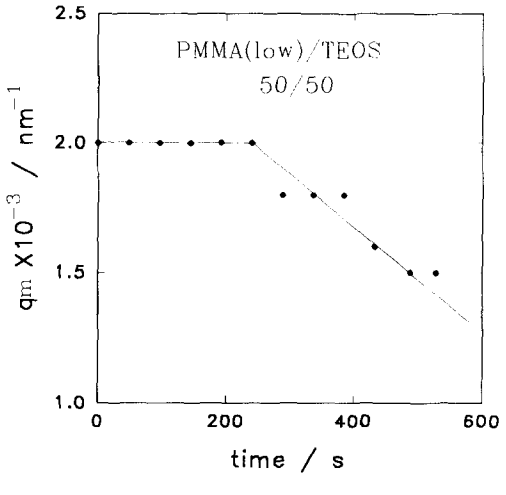

Figure 5 Wavenumber of the predominant concentration fluctuation in the system (q_m) as a function of time for the 50/50 low molecular weight PMMA/TEOS system

for the 50/50 (low) system that the predominant fluctuation wavenumber ($q_m = 2.0 \times 10^{-3}$ nm^{-1}) is initially constant, up to ~240 s after the demixing starts, and then decreases with time, as an indication of coarsening. Similar plots were obtained for 60/40 (low) ($q_m = 2.7 \times 10^{-3}$ nm^{-1}) and 50/50 (high) ($q_m = 2.0 \times 10^{-3}$ nm^{-1}) systems, but coarsening starts earlier in the last case.

Table 1 summarizes the light scattering results for all of the investigated PMMA/TEOS systems. Spinodal decomposition was observed for intermediary compositions for the low molecular weight PMMA system and also for those with higher PMMA content with high molecular weight. As estimated by D_{app} values, the mobility when SD phase separation initiated was higher for the 50/50 (low) system. The results in *Table 1* can be better understood with the qualitative representation in *Figure 1*. The arrows indicate mainly the reaction/solvent evaporation process. The solvent evaporation starts from a finite T_{eq}, since a considerable part of the reaction has already taken place, going from the initial ϕ(TEOS) value to the final silicate composition in the solid dry mixture.

In systems with low molecular weight PMMA, the NG mechanism was detected for the 20/80 PMMA/TEOS composition with a turbidity increase before any increase in viscosity could be noticed. Phase separation occurs before gelation. As pointed out by Nakanishi and Soga[13,14] the more time-consuming NG mechanism is favoured when viscosity is low. As mentioned before, clusters may be formed during the reaction. As THF evaporates, the demixing condition is achieved before the correlation length between silicate segments is high enough for percolation. If the TEOS concentration was much higher from the beginning, percolation would favour gelation before demixing, as depicted on the right of *Figure 1*. As the TEOS content decreased (and the relative PMMA content increased), gelation and phase separation seem to be almost simultaneous. The SD mechanism is favoured. The 60/40 system reaches the demixing condition after losing more mobility than the 50/50 system, as shown by the D_{app} values. For even lower TEOS content (70/30 PMMA/TEOS), SD was no longer observed, at least for low molecular weight PMMA. As shown in *Figure 1*, phase separation would be attained much later than gelation. Gelation here is probably related more to a decrease in mobility due to the high PMMA concentration at this point than to the formation of a percolated and chemically crosslinked silicate network. PMMA tends to form the matrix and the growth of the inorganic polymer by the condensation reaction leads to the formation of rather isolated silicate clusters which support the nucleation in the early stages of NG phase separation. The mobility is however too low and phase separation is not allowed to proceed with

Table 1 Phase separation mechanisms (NG or SD) and D_{app} values (in parentheses, nm^{2}s^{-1}) for PMMA/TEOS systems during solvent evaporation

PMMA M_w	PMMA/TEOS composition				
	20/80	40/60	50/50	60/40	70/30
Low	NG	NG	SD (1640)	SD (1360)	NG
High			SD (1120)		SD

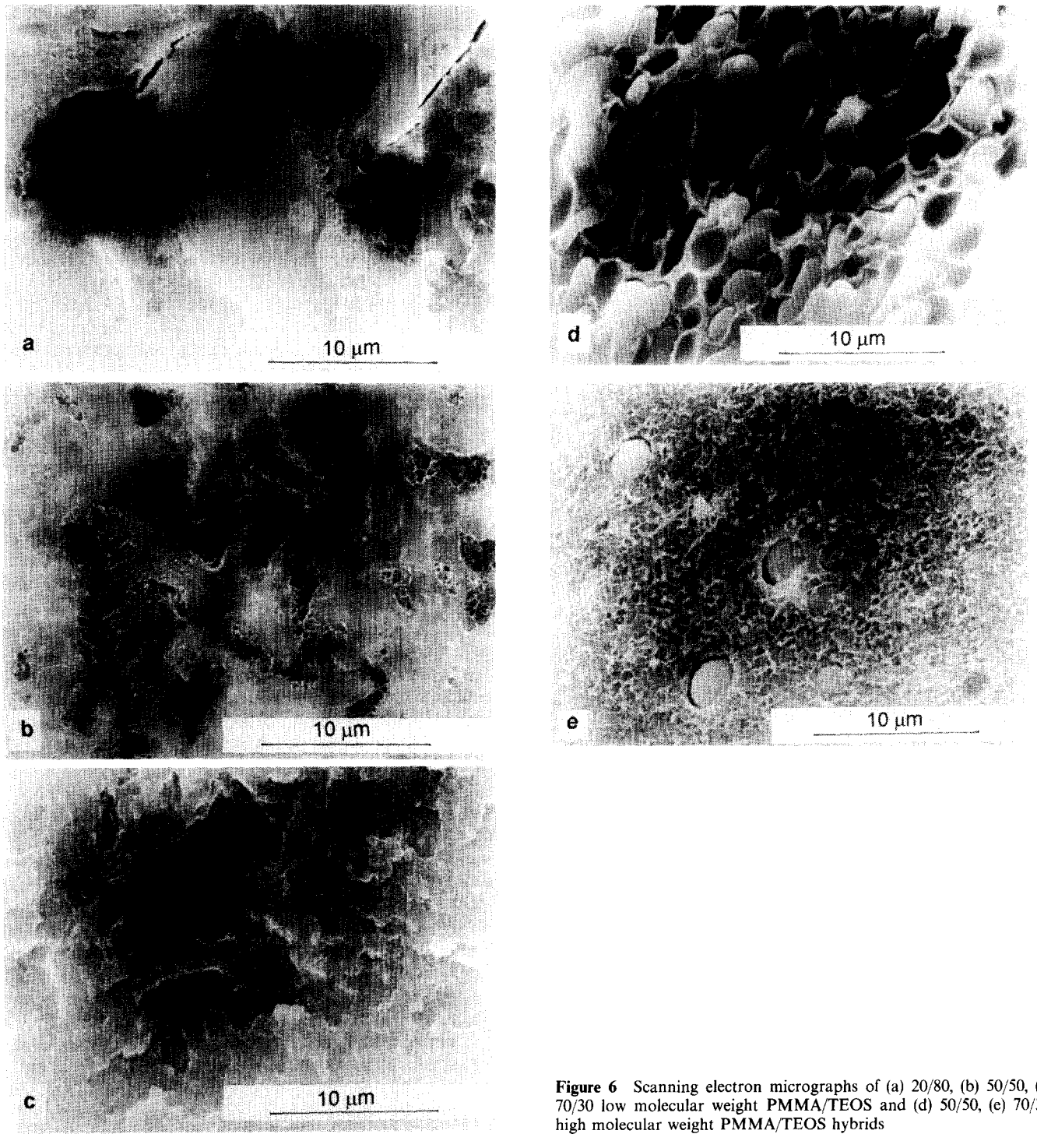

Figure 6 Scanning electron micrographs of (a) 20/80, (b) 50/50, (c) 70/30 low molecular weight PMMA/TEOS and (d) 50/50, (e) 70/30 high molecular weight PMMA/TEOS hybrids

the formation of larger domains. This accounts for the low opacity of the system. When high molecular weight PMMA was used, the viscosity of the system was higher from the start. During phase separation the mobility was lower as shown by the D_{app} values for 50/50 PMMA/TEOS solutions. Higher viscosity favoured the appearance of a scattered halo typical of SD even for 70/30 solutions.

Morphology after solvent evaporation

Scanning electron microscopy (SEM). *Figure 6* shows the morphology observed by SEM for PMMA/TEOS systems with different compositions, using PMMA with different molecular weights. With low molecular weight PMMA, the morphology was relatively homogeneous, especially at higher PMMA content. In 50/50 PMMA/TEOS systems, interconnected domains with irregular shapes could be observed as a result of coarsening of the structure obtained by spinodal decomposition. The fracture of systems with higher molecular weight PMMA shows separated spherical domains which easily detach from the homogeneous matrix. Although a SD mechanism was detected for the system, coarsening could continue to a later stage before gelation. Plots of q_m as a function of time showed a considerable decrease, from the beginning of phase separation, confirming that coarsening starts much earlier in this system. Using energy dispersive

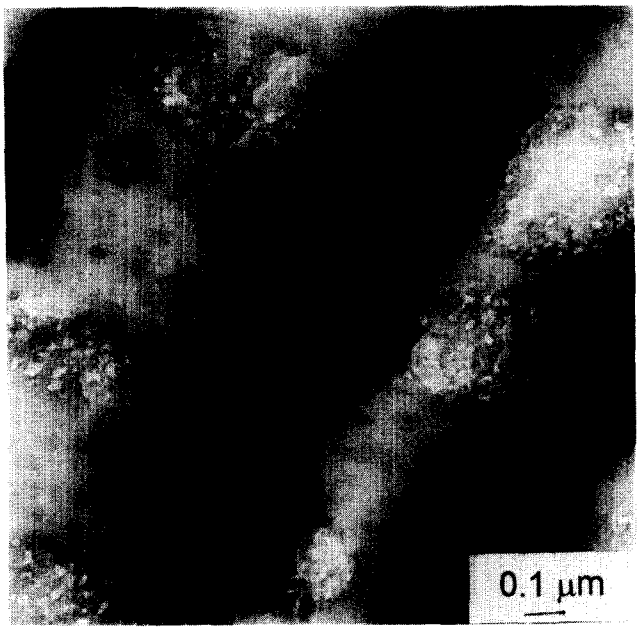

Figure 7 Transmission electron micrograph of 50/50 PMMA (low)/TEOS obtained with elastic electrons

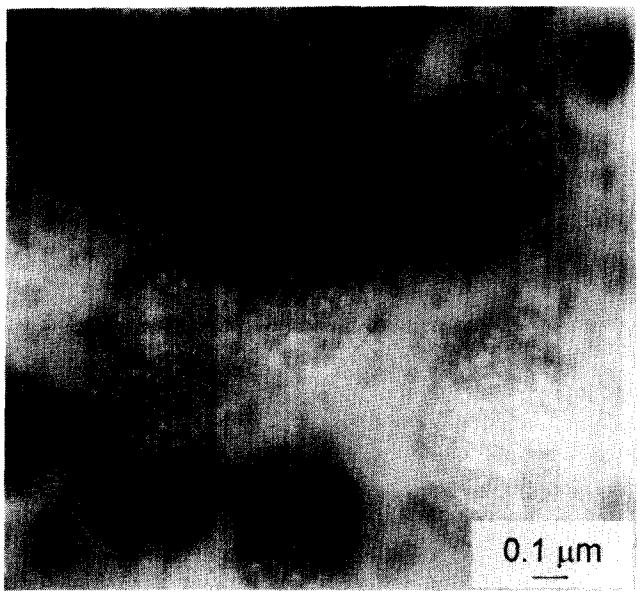

Figure 8 Transmission electron micrograph of 70/30 PMMA (low)/TEOS obtained with elastic electrons

X-ray analysis, the silicon-rich areas could be mapped as forming the silicate domains in the 50/50 PMMA/TEOS system.

Transmission electron microscopy (TEM). *Figures 7* and *8* show transmission electron micrographs obtained from thin cuts of PMMA/TEOS systems. With low molecular weight PMMA, domains with a fine globular internal structure could be seen in 50/50 and 70/30 PMMA/TEOS systems (*Figures 7* and *8*). Even when developed by different mechanisms, due to coarsening, the morphologies obtained in the later stages of phase separation are similar. Electron spectroscopic images (ESI) can be obtained if only inelastic electrons with energy losses characteristic for carbon or silicon are selected, the bright regions being those richer in the specific element. By this method, it was observed both for 50/50 and 70/30 that the domains are richer in silicate. Using electron energy loss spectra obtained selecting limited areas inside the dispersed domains or in the matrix (*Figure 9*), it was confirmed for both compositions that the matrix was not pure PMMA and the domains also contained PMMA. A different result can be seen in *Figure 10* for 20/80 PMMA/TEOS. The matrix contains practically no PMMA whereas in the dispersed domains silicon is below the detection limit. The domains are clearly separated from each other as a result of a phase separation by nucleation and growth. A lamellar structure is observed in the matrix (*Figure 11a*). ESI for this system is also shown in *Figures 11b* and *c*. The same lamellar structure can also be observed in the dispersed domains of 50/50 samples, which are rich in silicate, when high molecular weight PMMA is used (*Figure 12*). Higher PMMA molecular weight entropically favours phase separation. Coarsening starts earlier (q_m decreases from the beginning) and the dispersed domains are allowed to grow further. Larger domains than in the case of the

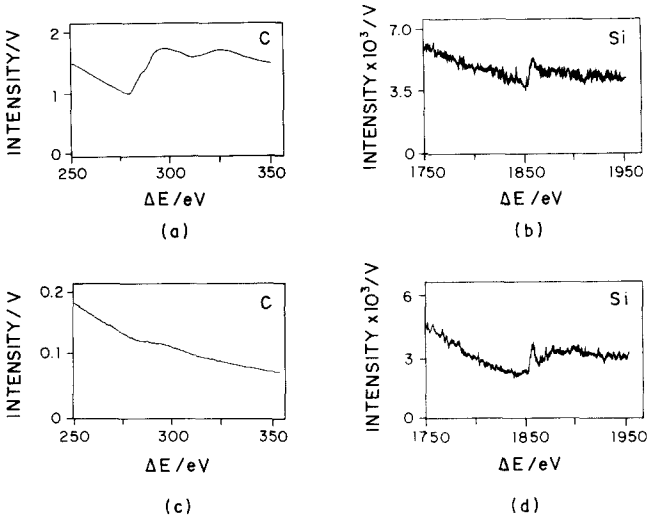

Figure 9 Electron energy loss spectra of (a, b) the matrix and (c, d) dispersed domains of a 50/50 PMMA (low)/TEOS hybrid in ΔE range characteristic for (a, c) carbon and (b, d) silicon

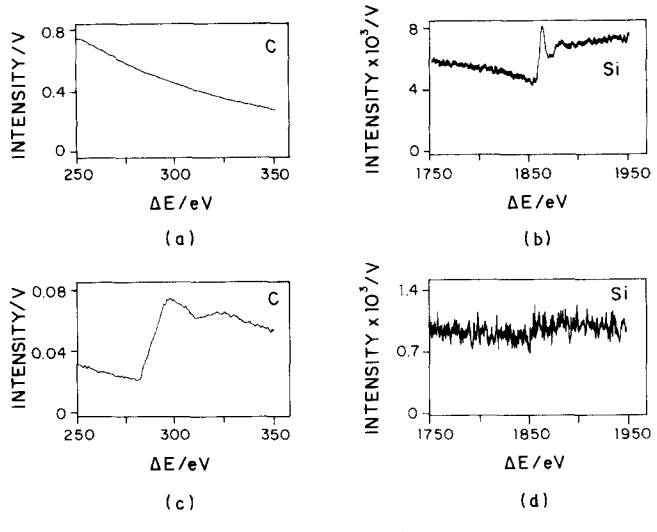

Figure 10 Electron energy loss spectra of (a, b) the matrix and (c, d) dispersed domains of a 20/80 PMMA (low)/TEOS hybrid in ΔE range characteristic for (a, c) carbon and (b, d) silicon

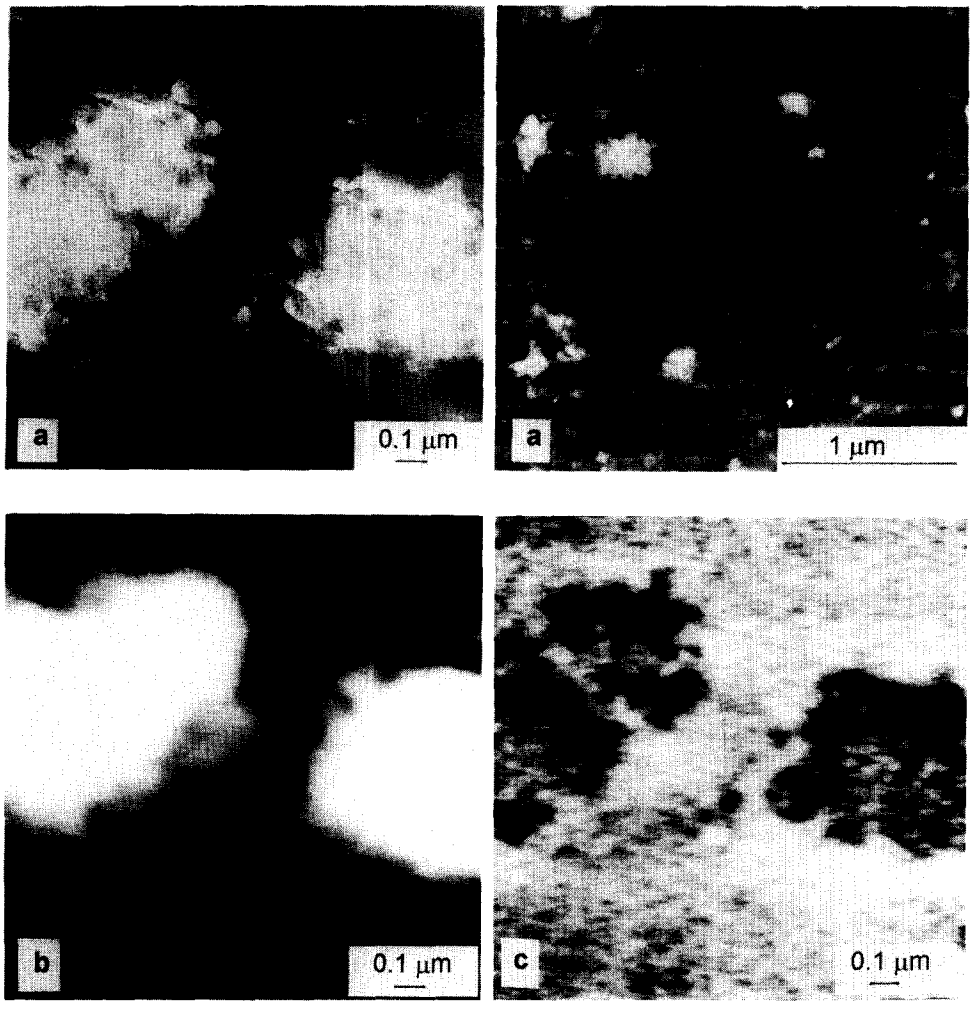

Figure 11 Transmission electron micrographs of 20/80 PMMA (low)/TEOS (a) obtained only with elastic electrons $\Delta E = 0$ and electron spectroscopic images (ESI) selective for (b) carbon ($\Delta E = 285$ eV) and (c) silicon ($\Delta E = 1839$ eV)

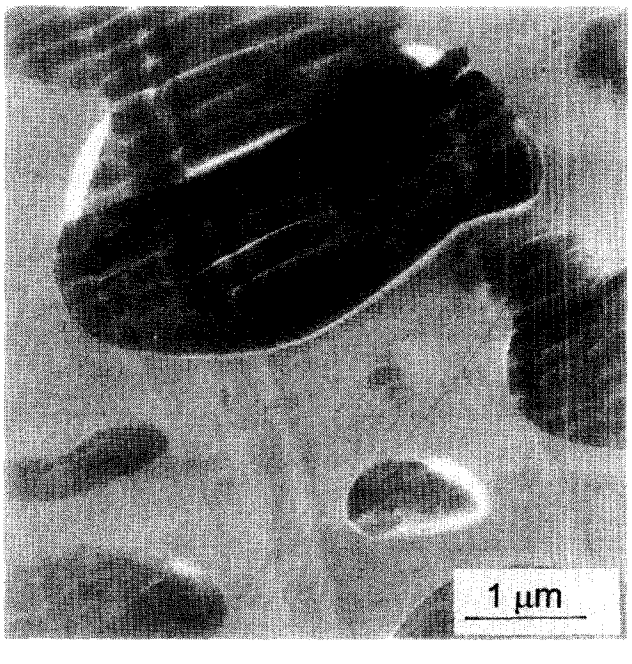

Figure 12 Transmission electron micrograph of 50/50 PMMA (high)/TEOS obtained with elastic electrons

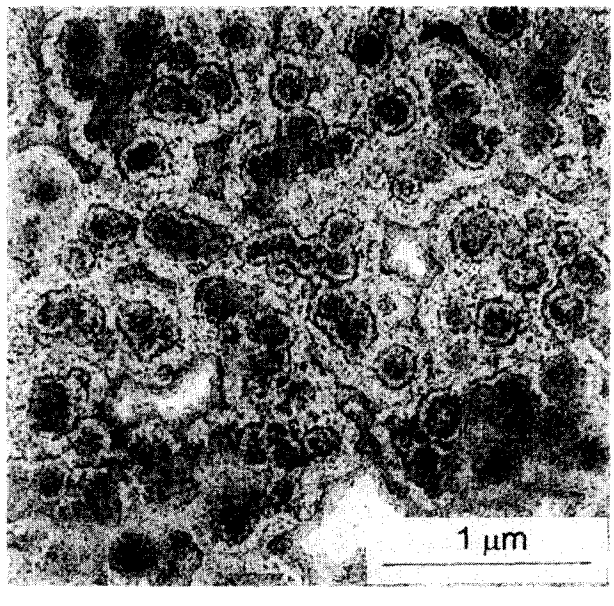

Figure 13 Transmission electron micrograph of 20/80 PMMA (low)/TEOS obtained only with elastic electrons from a different region of the sample in *Figure 11*, cut in the orthogonal direction

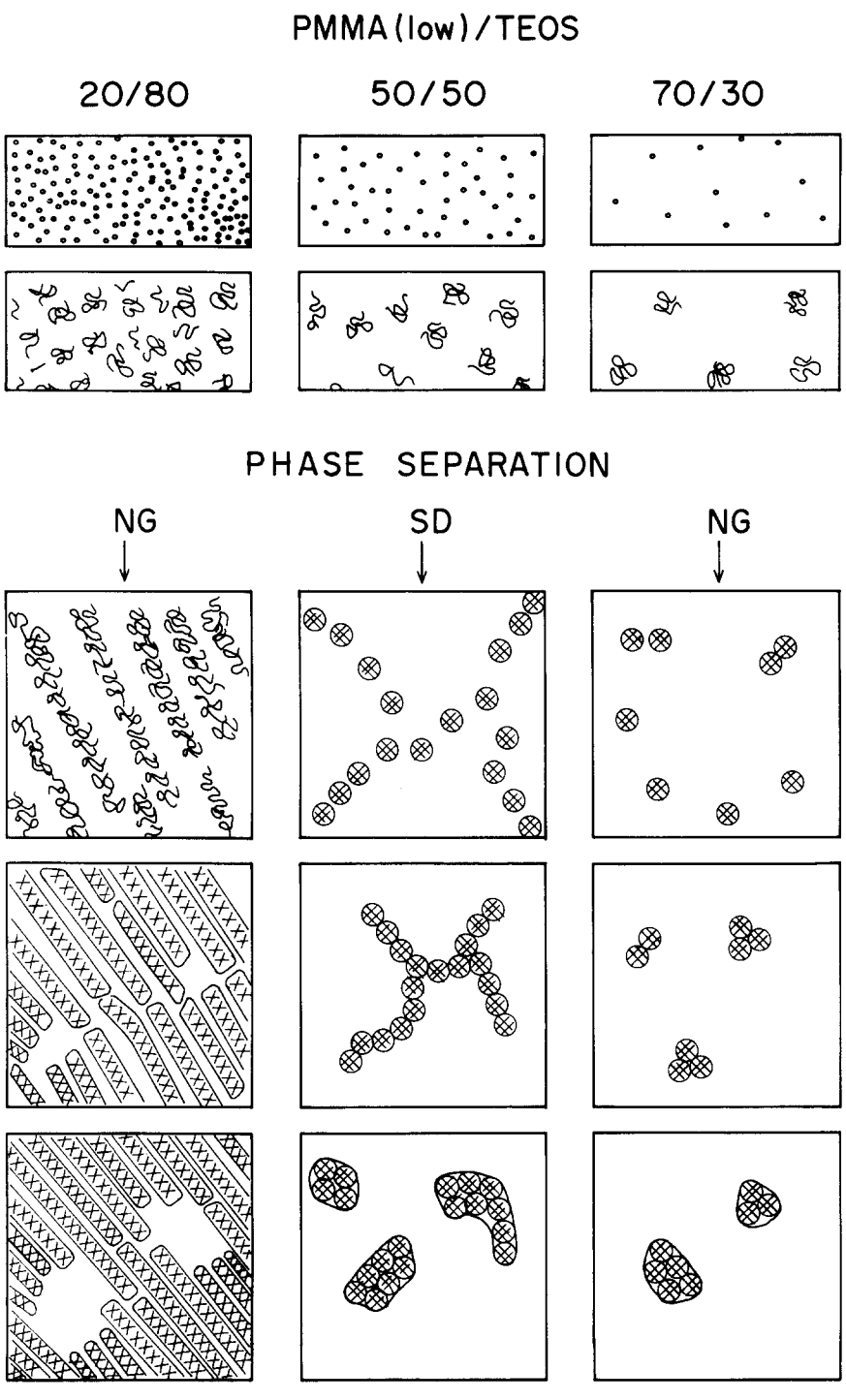

Figure 14 Sol–gel process with phase separation

same composition with low PMMA molecular weight were observed.

The finer morphology inside the separated phases—globular in the dispersed domains of 50/50 and 70/30 (low) PMMA/TEOS and lamellar in the matrix of 20/80 (low) PMMA/TEOS and in the domains of 50/50 (high) PMMA/TEOS—may have an explanation which is analogous to that described in the literature[34–36] for inhomogeneities in epoxide and phenolic thermoset resins or silicone. During the hydrolysis/condensation reactions, the SiO_2 polymer network is initially formed. The –OH and $-OCH_2CH_3$ group content in the network is progressively decreased and the miscibility between the growing inorganic polymer and other components in the mixture, especially the non-reactive PMMA and solvents, also decreases. An incipient cluster segregation may take place with a larger concentration of polar groups on the cluster surface. The reaction proceeds with intramolecular crosslinking, leading to micelles with a higher density of chemical links inside. Weaker links in the interfaces bond the micelles to one another as the solvent evaporates. Details of a morphology which could be related to the micelle formation can be observed in some segregated regions of a 20/80 PMMA/TEOS sample in *Figure 13*. As solvent evaporation goes on in the presence of PMMA the macroscopic phase separation commences according

to the different mechanisms (NG or SD). Even for those which follow the SD mechanism, a matrix/domain morphology may result due to coarsening and the domains still keep the details of the original microstructure. If the micelle concentration is high enough, as in the case of 20/80 PMMA(low)/TEOS, the micelles entangle leading to a cylindrical or lamellar morphology as in *Figure 11a*. The whole process is depicted in *Figure 14*.

REFERENCES

1 Manson, J. A. and Sperling, L. H. 'Polymer Blends and Composites', Plenum Press, New York, 1976
2 Wilkes, G. L., Orler, B. and Huang, H.-H. *Am. Chem. Soc., Div. Polym. Chem. Polym. Prepr.* 1985, **26**, 300–301
3. Huang, H.-H., Orler, B. and Wilkes, G. L. *Macromolecules* 1987, **20**, 1322
4 Schmidt, H. *J. Non-Crystalline Solids* 1985, **73**, 681
5 Chujo, Y. and Saegusa, T. *Adv. Polym. Sci.* 1992, **100**, 12
6 Morikawa, A., Iyoku, Y., Kakimoto, M. and Umai, Y. *J. Mater. Chem.* 1992, **2**, 679
7 Novak, B. M. *Adv. Mater.* 1993, **5**, 422
8 Philipp, G. and Schmidt, H. *J. Non-Crystalline Solids* 1984, **63**, 283
9 Okui, T., Okubo, T. and Nagamoto, H. ICOM 93, Heidelberg, 1993
10 Ulrich, D. R. *J. Non-Crystalline Solids* 1988, **100**, 174
11 Mackenzie, J. D. *J. Non-Crystalline Solids* 1988, **100**, 162
12 Landry, C. J. T., Coltrain, B. K., Landry, M. R., Fitzgerald, J. J. and Long, V. K. *Macromolecules* 1993, **26**, 3702
13 Nakanishi, K. and Soga, N. *J. Non-Crystalline Solids* 1992, **139**, 1
14 Nakanishi, K. and Soga, N. *J. Non-Crystalline Solids* 1992, **139**, 14
15 Novak, B. M., Ellsworth, M., Wallow, T. and Davies, C. *Am. Chem. Soc., Div. Polym. Chem. Polym Prepr.* 1990, **31**, 698
16 Ellsworth, M. W. and Novak, B. M. *J. Am. Chem. Soc.* 1991, **113**, 2756
17 Landry, C. J. T., Coltrain, B. K. and Brady, B. K. *Polymer* 1992, **33**, 1486
18 Landry, C. J. T., Coltrain, B. K., Wesson, J. A., Zumbulyadis, N. and Lippert, J. L. *Polymer* 1992, **33**, 1496
19 Ravaine, D., Seminel, A., Charbouillot, Y. and Vincens, M. *J. Non-Crystalline Solids* 1986, **82**, 210
20 Mauritiz, K. A., Jones, C. K. and Storey, R. F. *Polym. Mater. Sci. Eng.* 1988, **58**, 1079
21 Inoue, T. and Ougizawa, T. *J. Macromol. Sci.-Chem. A* 1989, **26**, 147
22 Hashimoto, T. in 'Current Topics in Polymer Science', Hanser, Munich, 1987, pp. 199–242
23 Brinker, C. J. *J. Non-Crystalline Solids* 1988, **100**, 31
24 Kunz, M., Möller, M., Heinrich, U.-R. and Cantow, H.-J. *Makromol. Chem., Macromol. Symp.* 1989, **23**, 57
25 Utracki, L. A. 'Polymer Alloys and Blends', Hanser, Munich, 1990
26 Inoue, T., Ougizawa, T., Yasuda, O. and Miyasaka, K. *Macromolecules* 1985, **18**, 57
27 Cahn, J. W. *J. Chem. Phys.* 1965, **42**, 93
28 Ohnaga, T. and Inoue, T. *J. Polym. Sci., Polym. Phys. Edn* 1989, **27**, 1675
29 Ohnaga, T., Chen, W. and Inoue, T. unpublished
30 Flory, P. J. 'Principles of Polymer Chemistry', Cornell University Press, Ithaca, New York, 1971
31 Stockmayer, W. *J. Chem. Phys.* 1943, **11**, 45
32 Martin, J. E. in 'Time-Dependent Effects in Disordered Materials' (Eds R. Pynn and T. Riste), Plenum Press, New York, 1987, pp. 425–449
33 de Gennes, P.-G. 'Scaling Concepts in Polymer Physics', Cornell University Press, Ithaca, New York, 1979
34 Batzer, H. 'Polymere Werkstoffe', Vol. 1, Georg Thieme, Stuttgart, 1987, pp. 668–714
35 Morgan, R. J. and Neal, J. E. O. *J. Mater. Sci.* 1977, **12**, 1966
36 Racich, J. L. and Koutsky, J. A. *J. Appl. Polym. Sci.* 1976, **20**, 2111